AAPS PharmSciTech (2022) 23: 57
DOI: 10.1208/s12249-022-02212-0

Research Article

The Optimized Formulation of Tamoxifen-Loaded Niosomes Efficiently Induced Apoptosis and Cell Cycle Arrest in Breast Cancer Cells

Iman Akbarzadeh,[1] Mahsa Farid,[2] Mehrnoosh Javidfar,[3] Negar Zabet,[4] Bahare Shokoohian,[1] Mandana Kazem Arki,[2] Anastasia Shpichka,[5,6,7] Hassan Noorbazargan,[8] Hamid Asadzadeh Aghdaei,[2] Nikoo Hossein-khannazer,[2,11] Peter Timashev,[5,6,9,11] Pooyan Makvandi,[10] and Massoud Vosough[1,11]

Received 28 September 2021; accepted 5 January 2022; published online 19 January 2022

Abstract. The aim, as proof of concept, was to optimize niosomal formulations of tamoxifen in terms of size, morphology, encapsulation efficiency, and release kinetics for further treatment of the breast cancer (BC). Different assays were carried out to evaluate the pro-apoptotic and cytotoxicity impact of tamoxifen-loaded niosomes in two BC cells, MDA-MB-231 and SKBR3. In this study, tamoxifen was loaded in niosomes after optimization in the formulation. The formulation of niosomes supported maximized drug entrapment and minimized their size. The novel formulation showed improvement in storage stability, and after 60 days only, small changes in size, polydispersity index, and drug entrapment were observed. Besides, a pH-dependent release pattern of formulated niosomes displayed slow release at physiological pH (7.4) and a considerable increase of release at acidic pH (5.4), making them a promising candidate for drug delivery in the BC treatment. The cytotoxicity study exhibited high biocompatibility with MCF10A healthy cells, while remarkable inhibitory effects were observed after treatment of cancerous lines, MDA-MB-231, and SKBR3 cells. The IC50 values for the tamoxifen-loaded niosomes were significantly less than other groups. Moreover, treatment with drug-loaded niosomes significantly changed the gene expression pattern of BC cells. Statistically significant down-regulation of *cyclin D*, *cyclin E*, *VEGFR-1*, *MMP-2*, and *MMP-9* genes and up-regulation of *caspase-3* and *caspase-9* were observed. These results were in correlation with cell cycle arrest, lessoned migration capacity, and increased caspase activity and apoptosis induction in cancerous cells. Optimization in the formulation of tamoxifen-loaded niosomes can make them a novel candidate for drug delivery in BC treatment.

KEY WORDS: nano drug-delivery; breast cancer; tamoxifen; apoptosis induction.

INTRODUCTION

Breast cancer (BC) is one of the most prevalent malignancies all over the world (1, 2) and is recognized as the leading cause of cancer-related mortalities in females aged 20 to 59 years (3). A huge body of literature has demonstrated the role of hormones in the development of BC and the efficiency of hormone antagonists (4, 5). Although, hormone therapy is still the most effective management of estrogen receptor (ER)—a positive type of BC; the treatment

[1] Department of Regenerative Medicine, Cell Science Research Center, Royan Institute for Stem Cell Biology and Technology, ACECR, Tehran, Iran.
[2] Gastroenterology and Liver Diseases Research Center, Research, Institute for Gastroenterology and Liver Diseases, Shahid Beheshti University of Medical Sciences, Tehran, Iran.
[3] Department of Genetic, Islamic Azad University, North Tehran Branch, Tehran, Iran.
[4] Department of Medicinal Chemistry, School of Pharmacy, Shahid Beheshti University of Medical Sciences, Tehran, Iran.
[5] World-Class Research Center "Digital biodesign and personalized healthcare", Sechenov First Moscow State Medical University, Moscow, Russia.
[6] Institute for Regenerative Medicine, Sechenov First Moscow State Medical University, Moscow, Russia.
[7] Yaroslav-the-Wise Novgorod State University, Veliky Novgorod, Russia.
[8] Department of Biotechnology, School of Advanced Technologies in Medicine, Shahid Beheshti University of Medical Sciences, Tehran, Iran.
[9] Chemistry Department, Lomonosov Moscow State University, Moscow, Russia.
[10] Istituto Italiano di Tecnologia, Centre for Materials Interface, viale Rinaldo Piaggio 34, Pontedera, 56025, Pisa, Italy.
[11] To whom correspondence should be addressed. (e–mail: nikookhannazer@gmail.com; Timashev.peter@gmail.com; masvos@Royaninstitute.org)

efficacy is considerably limited because of acquired endocrine resistance to this type of treatment (6–8). Therefore, there is an urgent need for applying novel molecular approaches to conquer the underlying mechanisms leading to endocrine resistance in this malignancy. As one of the most well-recognized hormone antagonists, tamoxifen citrate is currently prescribed for treating patients with ER-positive BC (9). Tamoxifen plays its role through interfering with cell proliferation and growth that making it a potent agent for BC treatment (10–12). Despite the oral bioavailability and first-pass metabolism in the liver and intestines, the plasma protein binding of tamoxifen and afimoxifene, particularly to albumin, is more than 99% (13). The peak serum level of tamoxifen happens 3 to 7 h after intake and reaching a steady stats level takes up to 16 weeks after regular daily administration. The American Cancer Society lists tamoxifen as a known carcinogen, stating that it increases the risk of some types of uterine cancer while lowering the risk of breast cancer recurrence (14). Besides, its long-term systemic use leads to life-threatening hepatotoxicity (as results of oxidative stress caused by reactive oxygen species), and increasing the risk of liver and endometrial cancers as well (15, 16). The above-mentioned issues lead scientists to develop novel methods for more targeted, controllable, and precise drug delivery system. Nanomedicine has appeared as an alternative and modern approach to overcome the current treatment drawbacks (17–21). Nanodrug-delivery platforms facilitated targeted delivery of medicinal products and can promote therapeutic efficacy and reduce undesirable side effects. In addition, targeted delivery and sustained release of medications, such as tamoxifen, improves drug pharmacokinetics (22–25). Niosomes are brilliant examples of pharmaceutical carriers that function as drug-encapsulating vehicles for targeted delivery of anticancer drugs within optimized and definite periods, from hours to weeks, in a sustained release manner (26–28). These nanocarriers can easily be constructed *via*self-assembly of non-ionic surfactants in a bilayer scale to generate vesicular structures, with or without cholesterol as an additive (29, 30). These nanoparticles have many advantages over conventional delivery methods comprising adequate stability, biocompatibility, biodegradability, and non-immunogenicity(31). Also, niosomes are more cost-effective and have easier storage of the nonionic surfactants than phospholipid-containing liposomes. Niosomes are pH-responsive materials. An acidic pH enhances the hydrolysis of the surfactant molecules in the periphery of the niosome, which results in a burst release of the loaded biomolecules (32, 33). The aim of the present study, as proof of concept, was to optimize niosomal formulations of tamoxifen in terms of size, morphology, encapsulation efficiency, and release kinetics. Different assays were carried out to evaluate the pro-apoptotic and cytotoxicity impact of tamoxifen-loaded niosomes in two BC cells, MDA-MB-231 and SKBR3.

MATERIALS AND METHODS

Materials

Tamoxifen citrate was obtained from the Iran Hormone Company (Tehran, Iran). The MDA-MB-231 and SKBR3 cell lines were provided by the Pasteur Institute of Iran (Tehran, Iran). Dialysis membranes (MWCO 12000 Da) and acetone were obtained from Sigma-Aldrich (St Louis, MO, USA). Ethanol (96%), chloroform, methanol, span20, span40, span60, span80, dimethyl sulfoxide (DMSO), isopropyl alcohol, Milli-Q water, sodium dodecyl sulfate (SDS), and cholesterol (Chol, purity > 98%) were all ordered from Merck (Darmstadt, Germany). Trypsin-EDTA, Trypan blue, RPMI-1640 Medium, DMEM (Dulbecco's modified eagle medium), PBS (phosphate-buffered saline), FBS (fetal bovine serum), MTT (dimethylthiazol-2-yl-)-2,5, and penicillin/streptomycin(PS) 100 × were purchased from Gibco (Grand Island, NY, USA). Annexin V-FITC flow cytometric kit was purchased from Affymetrix Biosciences (Santa Clara, CA, USA). Caspase 3 and caspase 9 kits were provided from Invitrogen (Camarillo, CA, USA). Finally, RNA extraction and cDNA synthesis kits were obtained from TransGene Biotech Co., Ltd. (Beijing, China) (Cat No. ER101-01 and AE301-02). All the chemicals and reagents which were used in this study were HPLC and/or analytical grade.

Preparation of Tamoxifen Citrate–Loaded Niosomes

Different niosomal formulations according to surfactant type and lipid to drug molar ratio were prepared through the thin film hydration method as described before. Tamoxifen citrate, 10 mg, and different spans (20, 40, 60, and 80) and various amounts of cholesterol (Table I) were meticulously weighted and dissolved in a chloroform/methanol mixture (9 mL; 2:1 v/v). The total mixture was evaporated in a rotary evaporator under reduced pressure at 60°C at 150 rpm for 30 min until a thin film was formed. Then, the dried thin layer was hydrated with a PBS solution (10 mL) adjusted to pH 7.2 at 60°C for 30 min, while being gently mixed at 120 rpm (Fig. 1a). Eventually, the formed niosomal suspension was sonicated (Hielscher up50H ultrasonic processor, Germany) for 7 min. To optimize the size of niosomes, all the variable parameters were adjusted accordingly.

Characterization of Tamoxifen-Loaded Niosomes

The particle size, zeta potential and polydispersity index (PDI) of niosomal formulations were determined at 25°C using a benchtop dynamic light scattering/electrophoretic light scattering system (Zetasizer Nano S90, Malvern Panalytical Ltd., Malvern, UK). Scanning electron microscopy (NOVA NANOSEM 450 FEI model) was utilized to analyze the surface morphology of the prepared niosomes. For imaging by SEM, a thin layer of gold or graphite is deposited on the surface to make the surface conductive, and fine samples spread on a conductive film such as aluminum and thoroughly dried.

Entrapment Efficiency

The suspension of tamoxifen citrate–loaded niosomes ($T_{n\text{-loaded}}$) was ultra-filtered for 20 min at 4000 *g* through an Amicon Ultra-15-membrane (MWCO 30,000 Da) (Eppendorf® 580R centrifuge, Germany). In the filtration process, drug-loaded niosomes remained in the upper

Table I. Composition of different tamoxifen citrate-loaded niosomal formulations

Formulation ID	Surfactant	Chemical name	Structure	HLB	Lipid/drug (M ratio)	Tamoxifen (mg)	Span (mg)	Cholesterol (mg)
F1	Span 20	Sorbitan monolaurate	$C_{18}H_{34}O_6$	8.60	10	10	46.6	52.0
F2	Span 40	Sorbitan monopalmitate	$C_{22}H_{42}O_6$	6.70	10	10	54.2	52.0
F3	Span 60	Sorbitan monostearate	$C_{24}H_{46}O_6$	4.70	10	10	58.00	52.0
F4	Span 80	Sorbitan monooleate	$C_{24}H_{44}O_6$	4.30	10	10	57.7	52.0
F5	Span 20	Sorbitan monolaurate	$C_{18}H_{34}O_6$	8.60	20	10	93.3	104.0
F6	Span 40	Sorbitan monopalmitate	$C_{22}H_{42}O_6$	6.70	20	10	108.4	104.0
F7	Span 60	Sorbitan monostearate	$C_{24}H_{46}O_6$	4.70	20	10	115.9	104.0
F8	Span 80	Sorbitan monooleate	$C_{24}H_{44}O_6$	4.30	20	10	115.4	104.0

*HLB*Hydrophilic–lipophilic balance; Lipid is the total amount of cholesterol and surfactant; Tamoxifen concentration (1 mg/ml); surf/chol (1:1 mol ratio); sonication time (7 min)

chamber, and the untrapped drug moved through the filter membrane. Then, the concentration of free drug (untrapped) was measured at the wavelength of 236 nm *via*UV-Vis spectrophotometry (Jasco V-530, Japan Servo Co. Ltd., Japan). Finally, Eq. (1) was used to calculate the entrapment efficiency (EE), in which, "**A**" refers to the amount of the

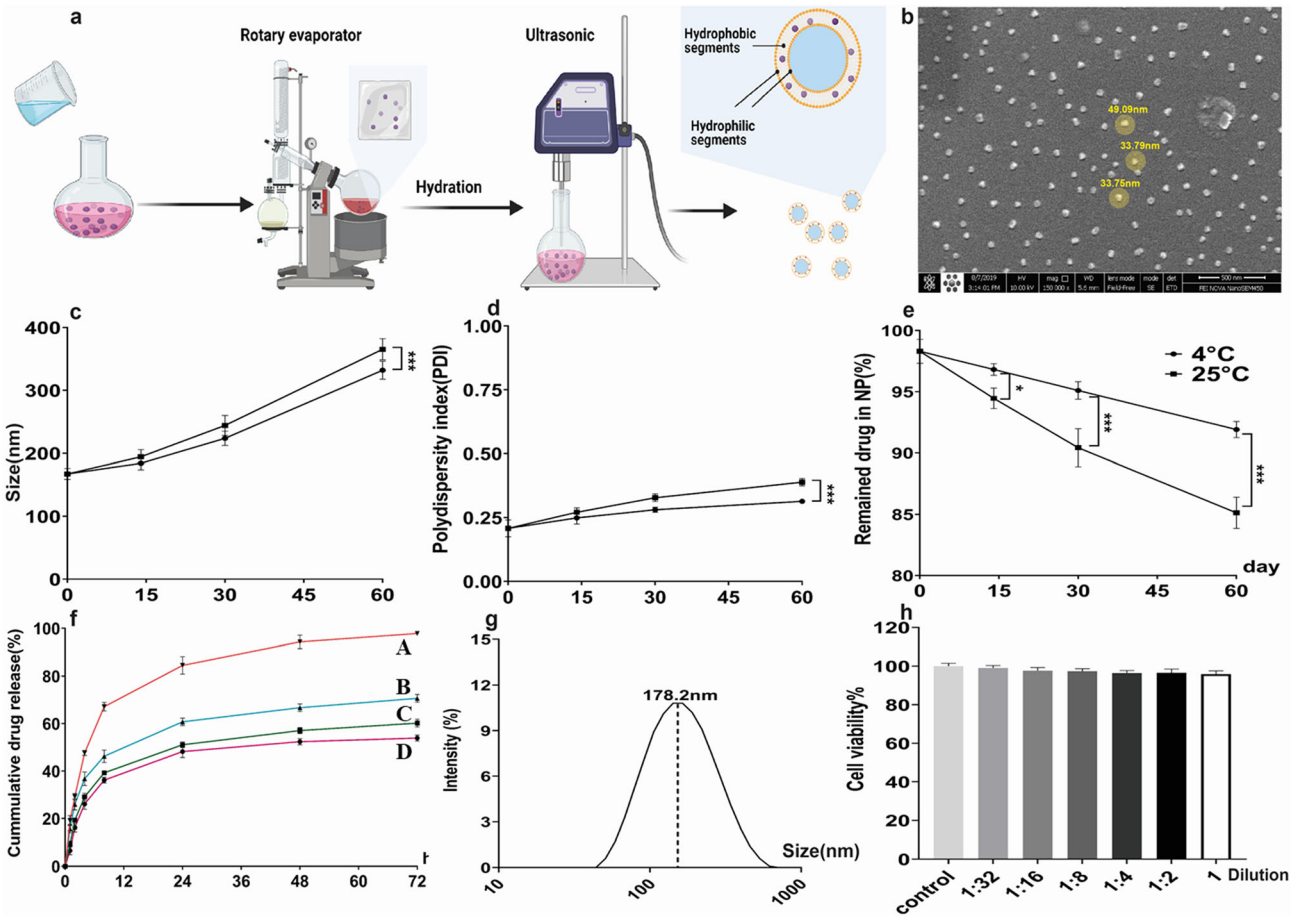

Fig. 1. Fabrication and characterization of a tamoxifen-loaded niosomes. **a** Schematic representation of fabrication and characterization of a tamoxifen-loaded niosomes; **b** scanning electron microscopy (SEM) image of the prepared span 80-based niosomes (F8-formulation based); **c** size alteration during storage and stability test of tamoxifen-loaded niosomes (F8 samples) after 2 months of storage at 4 ± 2°C and 25 ± 2°C, **d** polydispersity index, and **e** remaining drug in the niosomes (*p <0.05, **p <0.01, and ***p <0.001); **f** *In vitro* drug release profile of tamoxifen from different niosomal formulations including F8 formulations with pH 7.2 (f-D), 6.5 (f-C), and 5.4 (f-B) as well as the tamoxifen citrate solution (f-A); **g** Analysis of the particle size distribution of tamoxifen-loaded niosomes (F8-formulation) by dynamic light scattering (DLS);**h** Cell viability of MCF10A cells after a 72-h treatment with niosomes, The data are presented as mean ± SD, n = 5

initial drug used to load niosomes, and "**B**" denotes the amount of the free drug passed through the membrane.

$$\text{Entrapment efficiency}\ (\%) = [(\mathbf{A}-\mathbf{B})/\mathbf{A}] \times 100 \quad (1)$$

In Vitro Release Study and Kinetic Modeling

The release pattern of tamoxifen citrate from $T_{n\text{-loaded}}$ was assessed using the dialysis membrane method (MWCO 12000 Da). The samples (2 mL) were suspended in the release medium (50 mL), containing 0.5% SDS at pH 7.2, 6.5, and 5.4, using a magnetic stirrer at room temperature for 72 h. Then the amount of the released drug was evaluated using 236 nm UV-visible spectrophotometry.

To study the release kinetics as well as the mechanism of drug release from the $T_{n\text{-loaded}}$, the data of the drug release were mathematically analyzed based on the proportional models in kinetic models' equations, including zero-order kinetics, Higuchi model, first-order kinetics, and Korsmeyer–Peppas equation, by using linear form diagrams.

Evaluation of the Stability of Tamoxifen-Loaded Niosomes

To assess the stability of $T_{n\text{-loaded}}$, the prepared nanoparticles were stored for 2 months in two different conditions (25 ± 1°C (room temperature) and 4 ± 1°C (refrigerator temperature)/60% relative humidity (RH) ± 5% RH) and physical properties such as the size (nm), PDI, and EE (%) were evaluated at certain time points (14, 30, and 60 days).

MTT Assay

To evaluate the cytotoxicity of $T_{n\text{-loaded}}$, the cell viability assay was performed using the 3-(4,5-dimethylthiazol-2-yl)-2,5-diphenyltetrazolium bromide (MTT) dye reduction kit. In brief, MDA-MB-231, SKBR3, and MCF10A cell lines were cultured in 96-well plates at 1×10^4cells/well density. After overnight incubation, different concentrations of $T_{n\text{-loaded}}$, soluble tamoxifen (T_{aq}), $T_{aq.}$ combined with $T_{n\text{-loaded}}$ ($T_{aq+n\text{-loaded}}$), and finally, the empty niosomes as vehicles were added to the plates in eight replicates and incubated at 37°C for 48 and 72 h. Afterward, 100 μL of MTT (0.5 mg/ml in PBS) was added to the wells and incubated at 37°C for 4 h. Then, the supernatants were collected, and 100 μL of DMSO was added to each well. The formation of purple formazan crystals was determined *via* recording the absorbance at 570 nm by a microplate reader (Biotek Instruments, Winooski, VT, USA). Using Eq. (2), the percentage of cell viability for each treatment was calculated.

$$\text{Cell viability percentage} = (A_{treatment}-A_{blank})/(A_{control}-A_{blank}) \times 100 \quad (2)$$

Annexin-PI Flow Cytometry

The impact of treatment of MDA-MB-231 and SKBR3 cells with $T_{n\text{-loaded}}$ were studied by the Annexin V-FITC/PI double staining assay. In MDA-MB-231 and SKBR3 cells, apoptotic activity was quantified through apoptosis assay by flow cytometry. First, cells were seeded and cultured in 6-cm cell culture plates at a density of 5×10^5cells/well for 24 h (37°C, 5 % CO_2). Then, the cells in four different groups were treated with $T_{n\text{-loaded}}$, T_{aq}, $T_{aq+n\text{-loaded}}$, and vehicle (IC_{50} concentrations), for 72 h, and apoptotic cells were assessed by Annexin V-FITC/propidium iodide assay kit (Transgene Biotech, Beijing, China). The cells were centrifuged at 1000 rpm, followed by washing the pellet with PBS and its resuspension in 250 μL of binding buffer. Then, they were incubated for 10 min with 2 μL Annexin V-FITC followed by propidium iodide (PI) staining. After staining, the flow analysis by FACSCalibur was used to evaluate the samples within 1 h.

Quantitative Real-Time PCR

Sample Preparation and RNA Extraction

MDA-MB-231 and SKBR3 cells were cultured and treated in four different groups, treated with ($T_{n\text{-loaded}}$), (T_{aq}), ($T_{aq+n\text{-loaded}}$), and vehicle at the IC_{50} concentrations for 72 h. The total RNA of the treated cells was extracted by TriZol (Roche, Switzerland) according to the manufacturer's instructions. The quality and quantity of RNA were assessed through gel electrophoresis and Nanodrop 2000C (Thermo Fisher Scientific, Wilmington, DE, USA), respectively.

cDNA Synthesis and Quantitative RT-PCR

The cDNA libraries were generated, by mixing a random hexamer and oligo-dT primers as well as reverse transcriptase enzyme, utilizing the Prime Script II reverse transcriptase reagent (TaKaRa, Japan) in a 20 μl total reaction volume. Specific primers for target genes were designed with the Allele ID software version 7 (Premier Biosoft International, Palo Alto, CA, USA) and further blasted using NCBI Primer-BLAST. Table II shows the primer sequences used in this study. The real-time PCR amplification was carried out in a Light Cycler® 96 instrument (Roche, Germany) using SYBR Premix Ex Taq II (TaKaRa, Japan) to quantify the gene expressions. Relative quantification of the gene expression

Table II. Primers used in the quantitative real-time PCR

Gene	Primers
MMP2	F: 5'- F: TTGACGGTAAGGACGGACTC-3' R: 5'- CATACTTCACACGGACCACTTG -3'
CyclinD	F: 5'- CAGATCATCCGCAAACACGC-3′ R: 5'- AAGTTGTTGGGGCTCCTCAG-3'
b-actin	F: 5'- TCCTCCTGAGCGCAAGTAC-3' R: 5'- CCTGCTTGCTGATCCACATCT-3'
MMP9	F: 5'- GCACGACGTCTTCCAGTACC -3′ R: 5'- CAGGATGTCATAGGTCACGTAGC -3'
Casp3	F: 5'- CATACTCCACAGCACCTGGTTA-3′ R: 5'- ACTCAAATTCTGTTGCCACCTT-3'
Casp9	F: 5'-CATATGATCGAGGACATCCAG-3 R: 5'-TTAGTTCGCAGAAACGAAGC-3'
Cyclin E	F: 5'- CTCCAGGAAGAGGAAGGCAA-3′ R: 5'- TTGGGTAAACCCGGTCATCA-3'

levels was performed *via* normalizing to the *β-actin* (*ACTB*) gene as an internal control. The results were described as relative fold changes and compared with the control groups.

Caspase activity

The caspase 3 and caspase 9 enzyme activities in the samples (IC_{50} concentrations) retrieved from MDA-MB-231 and SKBR3 cell lines were assessed by the enzyme-linked immunosorbent assay (Roche, Germany) according to the manufacturer's instructions.

Cell Cycle Analysis

The cell proliferation assessment was accomplished using propidium iodide (PI) staining. Cells were seeded in 6-well plates (1×10^6 cells/well) and incubated overnight. The cells were washed three times with PBS (1000 μL) and treated with $T_{n\text{-loaded}}$ (IC_{50} concentrations) for 72 h. Following the incubation, the cells were fixed with 70% cold ethanol at $4^{\circ C}$ and stained with 500 μL of the PI solution (containing RNase) in the dark condition for 20 min at room temperature. Finally, the samples were analyzed by flow cytometry. All experiments were performed in three independent biological replications.

Scratch Assay

To investigate the anti-metastatic features of each formulation, the "wound-healing" assay was performed. Cells were cultured in a 6-well plate. The monolayer of cells was gently scratched and removed using a 200-μl pipette tip. The detached cells were washed twice with 1X PBS, and a fresh medium was added to the culture. The $T_{n\text{-loaded}}$ (IC_{50} concentrations) treated cells were incubated at 37°C, with 5% CO_2 to evaluate the migration capacity (wound healing test). After 72 h, the cells were imaged under a fluorescence microscope (Nikon Eclipse Ti, Nikon Instruments Inc., Melville, NY, USA) and compared with their pre-treatment condition.

Statistical Analysis

In the present study, the data were analyzed and plotted using GraphPad Prism, version 8 (GraphPad Software, San Diego, CA). The statistical analysis was carried out using two-way analysis of variances (ANOVA) test, followed by a post hoc Tukey. The data were shown as the mean ± standard deviation (SD) and $p<0.05$ was considered statistically significant. All experiments were performed in three independent biological replications.

RESULTS

Preparation of Tamoxifen-Loaded Niosomes

As shown in Table I, the impact of the surfactant type and lipid/drug molar ratio on the physicochemical properties and structure of generated niosomes were analyzed for eight different formulations. Using different commercial non-ionic surfactants of the span family (including 20, 40, 60, and 80), the impact of the surfactant type on the average size and efficiency of tamoxifen encapsulation was evaluated. Moreover, various formulations of niosomes, with different lipid/drug molar ratios along with various surfactant types, exhibited different sizes and PDI (results included in Table III). Interestingly, among the different span surfactants studied in this work, niosomal formulations containing span 80 appeared in the smallest size. Besides, between different span 80-based niosomal structures, those with the formulation of lipid/drug molar ratio of 10 (F4) were the appropriate niosomes vesicle size. Likewise, the final sample prepared by span 80 containing the lipid/drug molar ratio of 20 (F8) showed the highest level of tamoxifen encapsulation (98.30%) and was consequently considered for further investigations. As shown in Table III, formulations with the lipid/drug ratio of 10 were smaller in size than formulations with the lipid/drug ratio of 20, but in the context of the encapsulation efficiency, formulations with a lipid/drug ratio of 20 were more effective than formulations with the lipid/drug ratio of 10. Finally, F8 was chosen as the optimal formulation, because of its better characteristics in terms of the size and drug entrapment efficiency. The size of niosomes was measured by DLS, and the dimensions reflect the hydrodynamic diameter of the particles. The size of niosomes obtained by SEM was less than that obtained by Nano Zetasizer. The difference in the size measurement between SEM and DLS methods might be due to the drying process during the SEM imaging. In the other words, SEM represents the size of nanoparticles in a dried form (measures exact diameter of each particle), while DLS measures the hydrodynamic diameter of particles that includes core size plus any molecule attached or adsorbed on the surface of the particle including ions and water molecules (34, 35).

Morphological Characterization of the Optimized Niosomes

The SEM assessments confirmed that the niosomes had smooth surfaces as well as a uniform spherical morphology. Figure 1b demonstrates the SEM image of span 80-based niosomes following F8 formulation. The nanoniosomes had a diameter of <50 nm, and in reality, it was smaller than DLS-based results (Fig. 1g).

Physical Stability, PDI, and EE of Tamoxifen-Loaded Niosomes

After 2 months, the trend of alterations in the PDI and mean diameter revealed that at 4 ± 2°C, the rate of changes was slower than 25 ± 2°C (Fig. 1c and d). In addition, the retained drug amount in the niosomal formulations depicted a drug leakage rate of less than 10% at both temperatures (Fig. 1e). These data showed proper physical stability and effective formulation of generated niosomes. The niosome size and PDI values enhanced during the storage period. Furthermore, the storage stability of niosomes generated according to F8 formulation, at 4 ± 2°C was notably higher than that at 25 ± 2°C, which might be due to elevated hydrophobic rigidity of niosomes at the lower temperature. The differences in the particle size and PDI (Fig. 1d) between the samples stored at 4 and 25°C were only significant at day 60 ($p < 0.001$), while for the EE (remained drug in niosomes),

Table III. Niosomes size, polydispersity index (PDI), and EE% of tamoxifen citrate-loaded niosomes prepared by thin film hydration method

Formulation	Vesicle size (nm) mean ± SD)	Polydispersity index (mean ± SD)	EE (%) (mean ± SD)
F1	280.50±13.05	0.273±0.018	89.65±1.67
F2	227.80±7.84	0.198±0.012	90.88±2.12
F3	208.20±8.57	0.219±0.017	91.93±1.02
F4	139.20±6.66	0.228±0.007	94.86±0.73
F5	352.17±13.32	0.232±0.017	92.81±1.05
F6	281.73±15.68	0.224±0.045	92.78±1.20
F7	239.50±6.10	0.213±0.013	96.51±1.36
F8	167.47±8.64	0.208±0.033	98.30±0.97

Results are presented as mean ± SD, n=3

they were significant at days 14 ($p < 0.05$), 30 ($p < 0.001$), and 60 ($p < 0.001$) (Fig. 1e).

The *In Vitro* Release Pattern of Tamoxifen From Niosomes

Figure 1f illustrates the tamoxifen release pattern from niosomes. The release profiles showed that the niosomal formulations at different pH values have a specific controlled release pattern of tamoxifen over a period of time up to 24 h. During the first 24 h, more than 90% of the drug passed through the dialysis membrane into the phosphate buffer, containing 0.5% SDS. Niosomes composed of span 80 and cholesterol, generated according to the F8 formulation, at pH 7.2 showed the lowest tamoxifen release rate compare to the same formulation (F8) at other pH values (6.5 and 5.4). This is illustrated in Fig. 1f.

To analyze the release kinetics of the different formulations, multiple kinetic models were evaluated (36)(Table IV describes each model). In all models, the highest linear regression coefficient (R^2), close to 1, represents the most reliable kinetic model for the release pattern of each sample. As observed in Table IV, all samples (F8 formulation–based $T_{n\text{-loaded}}$ and $T_{aq.}$ at different pH values) in the Korsmeyer–Peppas model exhibited n <0.45, which demonstrated the Fickian diffusion release mechanism of this drug. This value was used to quantify the amount of tamoxifen molecules released from the niosomes (37).

In Vitro Cell Viability

To evaluate the cytotoxic and anti-proliferative effects of tamoxifen in four groups, i.e., empty niosomes (vehicle), the soluble drug ($T_{aq.}$), drug-loaded niosomes ($T_{n\text{-loaded}}$), and the combination of $T_{aq.}$ and $T_{n\text{-loaded}}$ ($T_{aq.}$ + $T_{n\text{-loaded}}$; 1:2 v/v), MTT assay performed on both breast cancer (BC) cell lines and healthy (normal) breast cell line. Treatment of both BC cell lines with $T_{n\text{-loaded}}$ (based on F_8 formulation) resulted in a significant decrease in cell viability compared to $T_{aq.}$ ($p < 0.001$) and the vehicle ($p < 0.001$) (Fig. 2c and d). This result could be related to the acidic environment around the cancer cells, which facilitates drug release from the $T_{n\text{-loaded}}$ and was also consistent with the drug release data at the acidic pH (Fig. 1f). Furthermore, the combination of $T_{aq.+\ n\text{-loaded}}$; 1:2 v/v had a higher inhibitory effect on the BC cells compared to the $T_{aq.}$ ($p < 0.001$) in both cell lines and $T_{n\text{-loaded}}$ ($p < 0.001$) in the MDA-MB-231 cell line. Thus, the treatment of cancer cells with $T_{n\text{-loaded}}$ and $T_{aq\ +\ n\text{-loaded}}$, showed a better cytotoxic effect compared to the T_{aq} treated cells. Therefore, the encapsulation of tamoxifen by niosomes appeared to enhance the anti-proliferative activity of the drug. Figure 2a and b show a significant decrease ($p < 0.05$) was observed in the IC50 values (Table V) of cancer cells after 72 h in the vehicle, $T_{aq.}$-, $T_{n\text{-loaded}}$-, and $T_{aq\ +\ n\text{-loaded}}$-treated groups compared to the 48-h treatment. The results also indicated that the vehicle had no significant toxicity on MCF10A cells after the 72-h treatment (Fig. 1h) that indicating the proper biocompatibility for application as a drug delivery system.

Quantitative Real-Time PCR

The relative expression analysis of crucial genes involved in apoptosis, angiogenesis, cell cycle, and tumor invasion pathways were assessed at the transcriptional levels (Figs. 3 and 5). It was demonstrated that in both MDA-MB-231 and SKBR3 cell lines, the expression levels of *caspase 3* and *caspase 9* were significantly increased in the groups, treated with soluble tamoxifen ($T_{aq.}$), tamoxifen-loaded niosomes ($T_{n\text{-loaded}}$), and a combination of both ($T_{aq.+\ n\text{-loaded}}$) compared to the untreated group. Besides, the differences between the ($T_{aq.\ +\ n\text{-loaded}}$) group *vs.* ($T_{n\text{-loaded}}$) group were significant ($p < 0.001$) for the MDA-MB-231 cells; however, the discrepancy was not significant ($p > 0.05$) in SKBR3 cells.

In MDA-MB-231 cells, significant downregulation of *Cyclin D* in the ($T_{n\text{-loaded}}$)- and ($T_{aq.\ +\ n\text{-loaded}}$)-treated groups were detected, compared to the control ($p < 0.05$ and $p < 0.001$ respectively) and between the ($T_{aq.}$)- *vs.* ($T_{aq.\ +\ n\text{-loaded}}$)-treated groups ($p < 0.01$) as well. Additionally, in SKBR3 cells, the ($T_{aq.}$)-, ($T_{n\text{-loaded}}$)-, and ($T_{aq.\ +\ n\text{-loaded}}$)-treated groups exhibited a significant decrease in the *Cyclin D* expression levels compared to the control group ($p < 0.05$, $p < 0.001$, and $p < 0.001$ respectively). In addition, a significant decrease was noted in the ($T_{n\text{-loaded}}$)- and ($T_{aq.\ +\ n\text{-loaded}}$)-treated groups in comparison with the (T_{aq})-treated group. ($p < 0.001$). Investigating the relative mRNA expression of *Cyclin E* in both the MDA-MB-231 and SKBR3 cells, we identified a significant decrease in the ($T_{n\text{-loaded}}$)- and ($T_{aq.+\ n\text{-loaded}}$)-treated groups *vs.* controls ($p < 0.01$ for MDA-MB-231 cells, and $p < 0.001$ for SKBR3 cells, respectively). The ($T_{n\text{-loaded}}$)- and ($T_{aq.\ +\ n\text{-loaded}}$)-treated groups showed declined levels compared to the ($T_{aq.}$)-treated group ($p < 0.01$) in MDA-MB-231 cells. Moreover, a significant decrease was noted in the ($T_{n\text{-loaded}}$)- and ($T_{aq.+\ n\text{-}}$

Table IV. Different kinetic models and their parameters for release pattern of tamoxifen from $T_{n\text{-loaded}}$

Release model	Equation	R^2 at 37°C			
		F8 (pH=7.2)	F8 (pH=6.5)	F8 (pH=5.4)	$T_{aq.}$ (pH=7.2)
Zero-order	$C_t=C_0+K_0t$	R^2=0.6886	R^2=0.7321	R^2=0.7461	R^2=0.7194
Korsmeyer–Peppas	$M_t/M_\infty=K_t^n$	R^2=0.8568	R^2=0.8915	R^2=0.9269	R^2=0.9187
		n*=0.4394	n*=0.3941	n*=0.3273	n*=0.3715
First-order	LogC=LogC0+K_t/2.303	R^2=0.7545	R^2=0.8138	R^2=0.8456	R^2=0.9756
Higuchi	$Q=K_H\sqrt{t}$	R^2=0.9809	R^2=0.9877	R^2=0.9846	R^2=0.9754

*Diffusion or release exponent
R^2 linear regression coefficient

$_{loaded}$)-treated groups in comparison with ($T_{aq.}$) ($p < 0.001$) in SKBR3 cells (Fig. 3). The expression of *MMP2 and MMP9* in MDA-MB-231 showed reduced levels in the $T_{aq.}$, $T_{n\text{-loaded}}$, and $T_{aq.\ +\ n\text{-loaded}}$ groups *vs.* controls ($p < 0.05$, $p < 0.001$, and $p < 0.001$, respectively) and between the ($T_{n\text{-loaded}}$)- and ($T_{aq.\ +\ n\text{-loaded}}$)-treated groups in comparison with ($T_{aq.}$) ($p < 0.01$). The decreasing trend of *MMP2* was also observed for SKBR3 cells in the mentioned groups ($p < 0.01$, $p < 0.001$, and $p < 0.001$ respectively). Furthermore, significantly decreased levels of *MMP9* were identified in the ($T_{n\text{-loaded}}$)- and ($T_{aq.+\ n\text{-loaded}}$)-treated groups, compared to the control group, and in the ($T_{n\text{-loaded}}$)- and ($T_{aq.\ +\ n\text{-loaded}}$)-treated groups, compared to ($T_{aq.}$)-treated cells in SKBR3 line ($p < 0.001$) (Fig. 5).

For *VEGFR1*, a significant reduction was observed in the expression levels in the ($T_{n\text{-loaded}}$)- and ($T_{aq.\ +\ n\text{-loaded}}$)-treated groups *vs.* control in both the MDA-MB-231 and SKBR3 cells ($p < 0.001$). The differences between the ($T_{aq.}$)-treated group *vs.* ($T_{n\text{-loaded}}$)- and ($T_{aq.\ +\ n\text{-loaded}}$)-treated groups were also significant ($p < 0.01$) for both the BC cell lines.

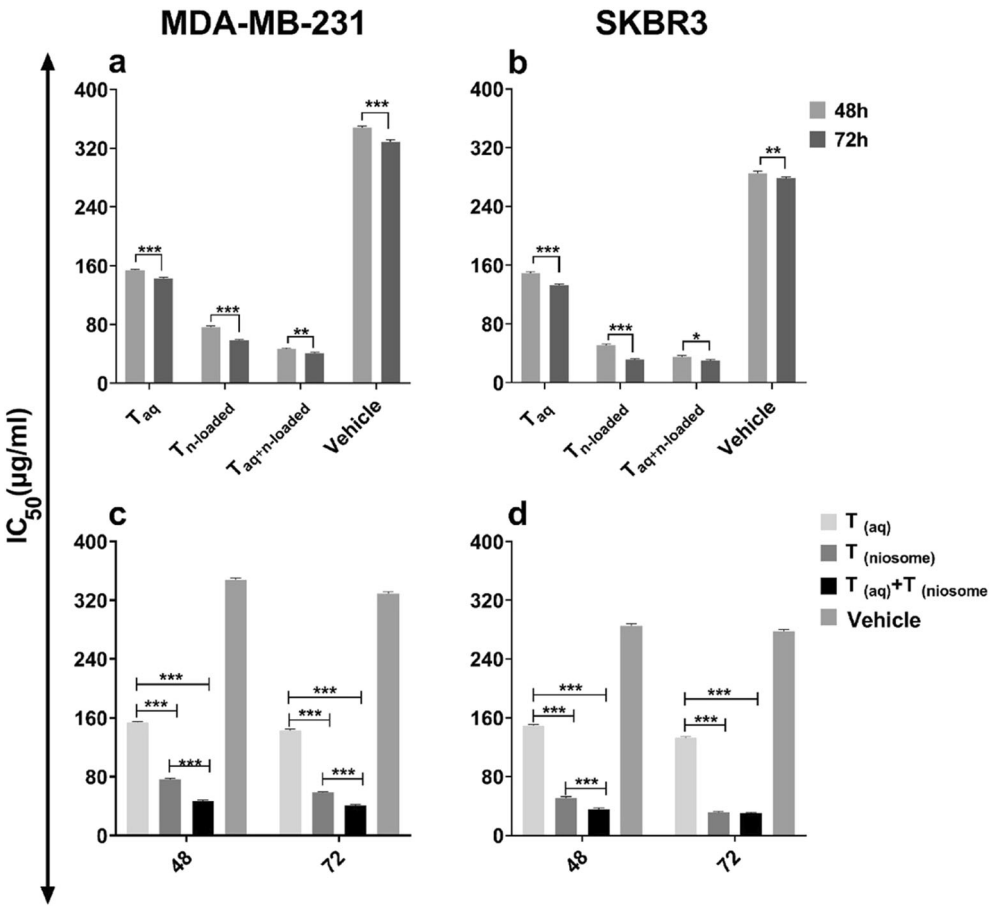

Fig. 2. **a**, **b** Comparison of IC50 in different groups at 48 and 72h in **a** MDA-MB-231 and **b** SKBR3 cell lines using MTT assay; **c**, **d** The effect of time on the IC50 values for different samples against **c** MDA-MB-231 and **d** SKBR3 cell lines using the MTT assay

Table V. IC50 calculation in different treated groups

Cell line	Time (h)	IC50 (μg/mL) of cancerous cells treated with			
		$T_{aq.}$	$T_{n\text{-loaded}}$	$T_{aq.\ +\ n\text{-loaded}}$ (1:2, v/v)	Vehicle
MDA-MB-231	48	153.85±1.35	76.39±1.50	46.87±1.22	347.98±2.29
	72	142.69±1.84	58.56±0.91	40.43±1.72	328.79±2.69
SK-BR-3	48	149.37±1.81	50.76±1.73	35.16±1.94	284.96±2.84
	72	132.651.64	31.25±1.20	29.87±1.33	277.83±2.21

Apoptosis Evaluation, Annexin-PI Flow Cytometry

Apoptosis of breast cancer cells after treatment was evaluated by double-staining the cells using annexin V, fluorescein isothiocyanate (FITC), and propidium iodide (PI). Apoptosis was induced after treatment of cancer cells at the IC50 concentration for each group and analyzed 72 h after incubation. Figure 4a and b quantified apoptosis in MDA-MB-231 cells and SKBR3 cells. The results demonstrated that encapsulation of tamoxifen in niosomes ($T_{n\text{-loaded}}$) and combined treatment of cells ($T_{aq.\ +\ n\text{-loaded}}$; 1:2 v/v) significantly enhanced the total apoptosis rate in both cell lines compared to the soluble form (T_{aq}). The analysis also showed that the apoptosis rates in the BC cell lines treated with ($T_{n\text{-loaded}}$) and ($T_{aq.\ +\ n\text{-loaded}}$) were significantly ($p < 0.001$) higher compared to the (T_{aq}) and control groups ($p < 0.001$) (Fig. 4a and b). The results were also consistent with the MTT assay results.

Cell Cycle Assessment

The impacts of treatment with $T_{aq.}$ and $T_{n\text{-loaded}}$ on the cell cycle in different groups were investigated using flow cytometry (Fig. 4c and d). The treatment with ($T_{n\text{-loaded}}$) and combined treatment group ($T_{n\text{-loaded}}$ and $T_{aq.\ +\ n\text{-loaded}}$; 1:2 v/v) resulted in shifting towards a sub-G1 phase of the cell cycle in both studied BC cells, i.e., MDA-MB-231 cells: 11.885 % for $T_{n\text{-loaded}}$, and 23.575 % for $T_{n\text{-loaded}}$ and $T_{aq.\ +\ n\text{-loaded}}$; SKBR3 cells: 20.750% for $T_{n\text{-loaded}}$, and 33.370% for $T_{n\text{-loaded}}$ and $T_{aq.\ +\ n\text{-loaded}}$. These trends were in association with the enhanced apoptosis rate, observed in MDA-MB-231 and SKBR3 cells discussed in the previous section.

Scratch Assay

Scratch assay was employed to pursue the effect of treatment with ($T_{aq.}$), ($T_{n\text{-loaded}}$), ($T_{aq.\ +\ n\text{-loaded}}$), and vehicle

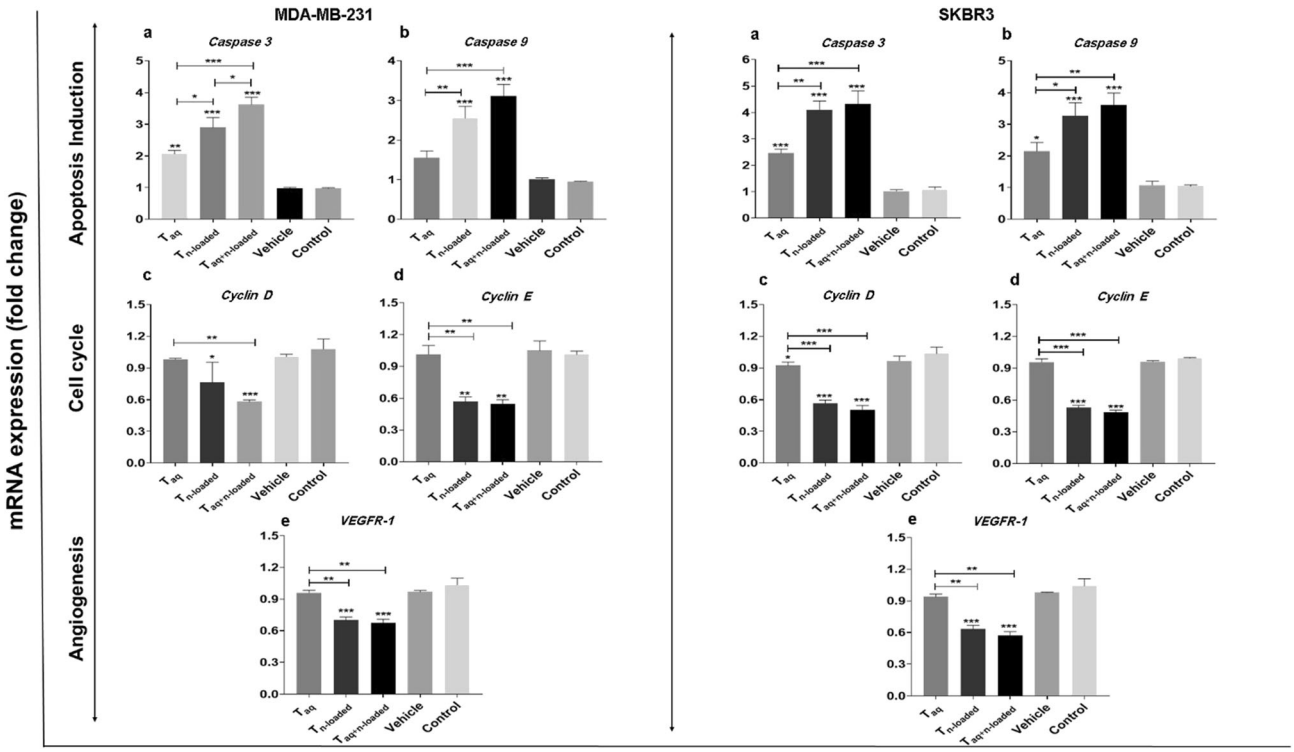

Fig. 3. The relative mRNA expression evaluation. **a**, **b** *Caspase 3* and *caspase* 9, **c**, **d** *CyclinD*, and *CyclinE*, and **e** *VEGFR-1* genes in MDA-MB-231 and SKBR3 cells after treatment. The $T_{aq.+\ n\text{-loaded}}$ treatment refers to the 1:2 mixture of the tamoxifen solution (T_{aq}) and tamoxifen-loaded niosome ($T_{n\text{-loaded}}$). The vehicle is the niosomal formulation without drug encapsulation. The IC50 was used for each sample; (*p <0.05, **p <0.01, and ***p <0.001).

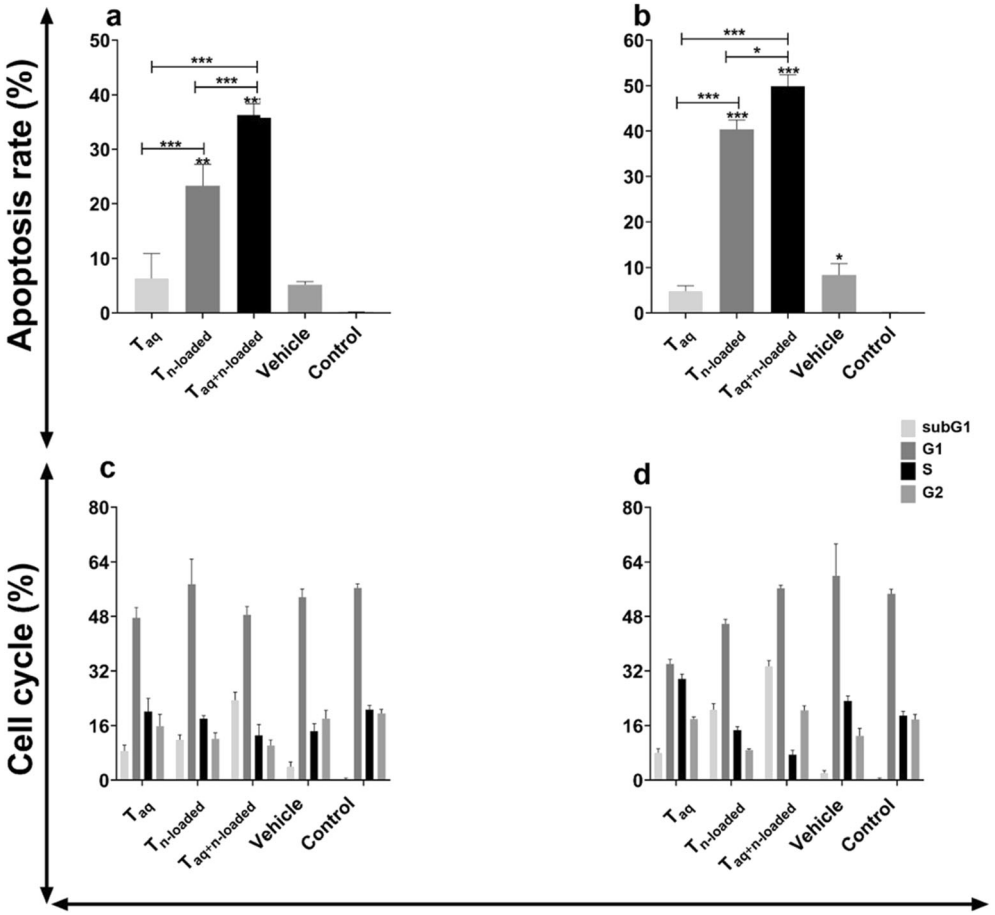

Fig. 4. **a**, **b** The quantitative apoptosis rate analysis of **a** MDA-MB-231 and **b** SKBR3 cells after treatment; **c**, **d** Cell cycle analysis of different samples for **c** MDA-MB-231 and **d** SKBR3 cells (*p <0.05, **p <0.01, and ***p <0.001)

groups on the motility and migration capacity of the MDA-MB-231 and SKBR3 cells. A notable reduction ($p < 0.001$) was observed in the percentage of the migrated cells in $T_{aq.\ +\ n\text{-loaded}}$- and $T_{n\text{-loaded}}$-treated groups compared to the $T_{aq.}$ and control groups (Fig. 5).

Caspase Activity

Figure 6 displays the comparison of the caspase 3 and 9 activities. In the MDA-MB-231 cells, the similar activity pattern of both caspase 3 (Fig. 6a) and caspase 9 (Fig. 6c) indicated the same trend. The caspase activity in the groups treated with $T_{aq.}$, $T_{n\text{-loaded}}$, and ($T_{aq.\ +\ n\text{-loaded}}$) revealed significantly increased caspase 3 activity levels compared to the control group ($p < 0.001$). This increased level of activity in the $T_{aq.}$-, $T_{n\text{-loaded}}$-, and $T_{aq.\ +\ n\text{-loaded}}$-treated groups were also significantly higher than the vehicle group (all p values were less than 0.05). Likewise, significant upregulation of the caspase 3 activity was observed in the ($T_{aq.\ +\ n\text{-loaded}}$)-treated group, compared to the $T_{aq.}$ and ($T_{n\text{-loaded}}$) groups ($p < 0.05$).

For the SKBR3 cells, the ($T_{n\text{-loaded}}$)- and ($T_{aq.\ +\ n\text{-loaded}}$)-treated groups displayed a significant increase in the caspase 3 activity, compared to the control group (both $p < 0.001$). Further, the caspase 3 activity (Fig. 6b) in these two groups was significantly incremented in comparison with the cells treated with only niosomes ($p < 0.001$). A considerable increase in the caspase activity observed in ($T_{n\text{-loaded}}$)- and ($T_{aq\ +\ n\text{-loaded}}$)-treated groups *vs.* T_{aq}-treated cells ($p < 0.001$).

For the caspase 9 activity (Fig. 6d), upregulated levels were seen in the T_{aq}-treated group in comparison with vehicle-treated cells ($p < 0.01$). The ($T_{n\text{-loaded}}$)-treated group also showed a significant elevation in the caspase 9 activity compared to the vehicle and the $T_{aq.}$-treated groups ($p < 0.001$, $p < 0.001$). Moreover, the caspase 9 activity in the $T_{aq.\ +\ n\text{-loaded}}$-treated group was significantly higher than the levels of caspase 9 in the vehicle, $T_{aq.}$, and $T_{n\text{-loaded}}$-treated groups (p values < 0.001, < 0.001, and $p < 0.05$ respectively).

DISCUSSION

One of the major challenges in the efficient treatment of breast cancer is effective and targeted drug delivery. The unwanted cytotoxicity is the main side effect of chemotherapy that limits the therapeutic effects (38, 39). Recent studies indicated that niosomes could be a promising tool for consistent and targeted drug delivery (4). Niosomes are synthetic nanoscale carriers for drug delivery, in which the medication is localized inside the nano vesicular structure. Niosomes primarily consist of an aqueous core encompassed by bilayer, comprised of cholesterol and one or more non-

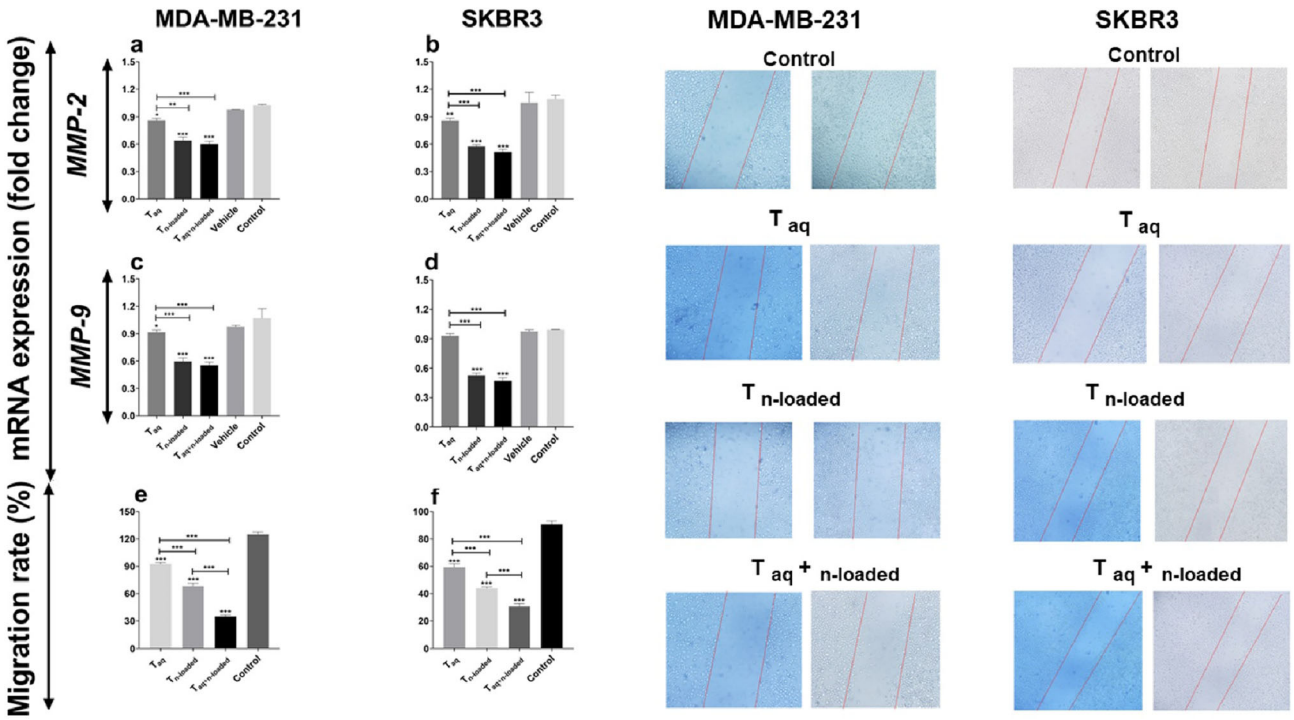

Fig. 5. The relative mRNA expression of **a**, **b** *MMP-2* and **c**, **d** *MMP-9* genes in MDA-MB-231 and SKBR3 cells after treatment. The $T_{aq.\ +\ n\text{-loaded}}$ refers to the 1:2 mixture of tamoxifen solution ($T_{aq.}$) and tamoxifen-loaded niosome ($T_{n\text{-loaded}}$). The vehicle is the niosomal formulation without drug encapsulation. The IC50 data was used for each sample; **e**, **f** The migration rate in wound healing test quantified in both cell lines after treatment with ($T_{aq.}$), ($T_{n\text{-loaded}}$), and ($T_{aq.\ +\ n\text{-loaded}}$) and presented as bar plots. (*p <0.05, **p <0.01, and ***p <0.001); **g**, **h** Wound healing test was used to evaluate the migration capacity of cancer cells under treatment of different formulations. Magnifications of the images are 10×

ionic surface-active agents (40, 41). Niosomes are more cost-effective and stable than liposomes. As a result, researchers were encouraged to apply niosomes in their studies. Niosomes are biocompatible, biodegradable, non-toxic, non-immunogenic, and non-carcinogenic nanoparticles. These features have made them promising carriers for sustained-release of drugs (41–43). In this study, we evaluated the impact of optimizing certain factors such as lipid:drug molar ratio and type of surfactant on size, PDI, and entrapment efficiency of niosomal formulations. The type and amount of each substance determine the physicochemical characteristics of the final product. The results of the synthesis of niosomes showed that the formulations with span 80 and lipid: drugs molar ratio (10 and 20) were resulted in suitable niosomes in terms of size, PDI and EE criteria, which is due to the increase in hydrophobic chain length in the structure of span 80 surfactant compared to span 20. The interaction of the tamoxifen encapsulated in the structure of the niosome with cholesterol and hydrophobic surfactant chains are the other factors (44). In niosomal structures, due to the hydrogen bonds between the hydroxyl groups and the alkyl chain of the surfactant, an interaction is established between cholesterol and the surfactant, which leads to the fluidity of the bilayer chains by increasing the vesicle transfer temperature and improving stability (4, 45–47). Cholesterol can also have a stabilizing effect due to its distribution between the two layers of the niosome membrane and increasing the entrapment efficiency (48–50). Examination of SEM microscope images showed differences in the size of niosomal structures compared to "Nano zetasizer" results. One of the reasons for the difference observed in the results is the drying of the samples in the process of preparation for SEM imaging. In DLS setting, the niosomes are hydrated, so that their hydrodynamic diameter is measured. Hydrodynamic diameter consists of the nucleus plus any molecule attached on the surface (ions and water) (51–53). Studies have confirmed that niosomes have the ability to control drug release in a two-phase process (54–56). Initially, the drug is released from the niosomal structure rapidly, and then, as the rate decreases, the release is controlled. In this process, the burst release happens due to the release of the drug from the outer surface of the niosomes, while the second phase seeks to release the drug through the bilayer membrane of the niosomes (55, 57). Stability study of niosomal structures showed that the mean diameter of the optimal formulation increased during storage time. Also, the particle size stored at 25°C was much larger than those stored at 4°C, and in addition, the EE% of the drug was reported to be lower at 25°C. It may be related to higher fluidity of lipid vesicles at higher temperature and leads to high drug leakage. Further, application of cholesterol in the structure of niosomes enhanced its performance in terms of EE%, storage time, permeability, and stability (58).

In the present study, we fabricated a niosome-based vehicle for the delivery of tamoxifen to improve the cytotoxicity effect and apoptosis induction. The treatment with ($T_{n\text{-loaded}}$ and ($T_{aq.\ +\ n\text{-loaded}}$) resulted in decreased viability and reduced the relative expression of *MMP2*, *cyclin D*, and *cyclin E*. This treatment blocked the cell cycle and induced apoptosis in the MDA-MB-231 and SKBR3 cells. The treatment with tamoxifen-loaded niosomes also

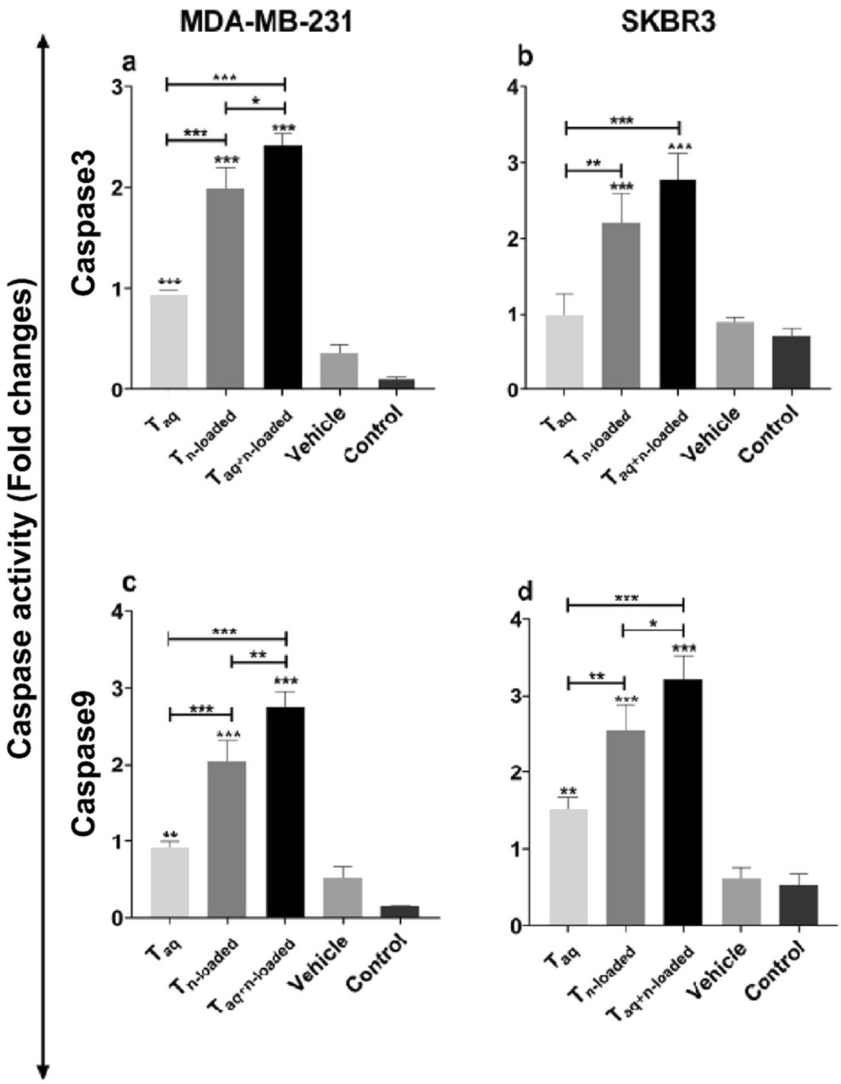

Fig. 6. Caspase activity in different treated groups. **a**, **b** Caspase 3 and **c**, **d** caspase 9 activity levels for MDA-MB-231 and SKBR3 cell lines (*p <0.05, **p <0.01, and ***p <0.001)

increased the *caspase 3* and *caspase 9* mRNA expression and activity as well. Our results showed that the cytotoxic effects of tamoxifen-loaded niosomes were significantly higher than those in the control group. Birangi *et al.*(12) and Kanaani *et al.*(59) also showed that niosomal formulation of anticancer drugs could increase the cytotoxicity effects. It was also indicated that niosomal formulation could increase apoptosis rate and block migration capacity of BC cells (11). Moreover, it was shown that niosomes could effectively entrapped in cancer cells through phagocytosis and directly deliver the loaded therapeutics to them and thereby decreasing major side effects (4, 59). As a result, it could provide a sustained release of the drug and lower the toxicity for the normal neighboring cells.

The cell cycle and apoptosis induction analysis indicated that the effect of treatment with the niosome-loaded drug was higher than that of soluble aqueous tamoxifen. In consistence with the previous studies, this might be because of the structural characteristics of niosomes (4, 60), in which the presence of cholesterol could cause structural stability and integrity of niosomes. Cholesterol is one of the crucial factors in the entrapment of tamoxifen and could control the release pattern of the drug (56, 60).

Altogether, our data have shown that tamoxifen-loaded niosomes can decrease the proliferation rate and induce cell cycle arrest and apoptosis in BC cell lines. However, more investigations are recommended to explore the *in vivo* side effects of niosomes and develop more practical protocols. In conclusion, our study indicated that tamoxifen-loaded niosomes have greater cytotoxicity effects and apoptosis induction compared to soluble aqueous tamoxifen.

AUTHOR CONTRIBUTION

I.A. and M.F. performed the experiments and data collection and drafted the manuscript. M.J., N.Z., B.S., M.K.A, P.T., N.H., and P.M. and contributed to the development of the concept, study design, and critically reviewed the manuscript. A.S., H.N., and H.A.A. contributed to study

design, data collection, and data analysis and drafting the results. M.V. developed the concept, contributed to data analysis, critical reviewing and approval of the manuscript, and financially supported the project.

FUNDING

This work was partly supported by the Bahar Tashkhis Teb, (BTT9903) and the Ministry of Science and Higher Education of the Russian Federation within the framework of state support for the creation and development of World-Class Research Centers "Digital biodesign and personalized healthcare" (N. 075-15-2020-917).

DECLARATIONS

Conflict of interest The authors declare no competing interests.

REFERENCES

1. Jia Y, et al. KLF4 overcomes tamoxifen resistance by suppressing MAPK signaling pathway and predicts good prognosis in breast cancer. Cell Signal. 2018;42:165–75.
2. Sarhadi M, Aryan L, Zarei M. The estrogen receptor and breast cancer: a complete review. CRPASE: Transactions of Applied Sciences. 06(04):309–14
3. Siegel RL, Miller KD, Jemal A. Cancer statistics. CA Cancer J Clin. 2016;66(1):7–30.
4. Shaker DS, Shaker MA, Hanafy MS. Cellular uptake, cytotoxicity and in-vivo evaluation of Tamoxifen citrate loaded niosomes. Int J Pharm. 2015;493(1-2):285–94.
5. Ferlay J, et al. Cancer incidence and mortality worldwide: sources, methods and major patterns in GLOBOCAN 2012. Int J Cancer. 2015;136(5):E359–86.
6. Schmid P, et al. Fulvestrant plus vistusertib vs fulvestrant plus everolimus vs fulvestrant alone for women with hormone receptor–positive metastatic breast cancer: the MANTA phase 2 randomized clinical trial. JAMA Oncol. 2019;5(11):1556–63.
7. Hanker AB, Sudhan DR, Arteaga CL. Overcoming endocrine resistance in breast cancer. Cancer Cell. 2020;37(4):496–513.
8. Molani S, Madadi M, Williams DJM. Investigating the effectiveness of breast cancer supplemental screening considering radiologists' bias. 2020. medRxiv, https://doi.org/10.1101/2020.12.16.20248373.
9. Ibrahim AB, et al. Evaluation of tamoxifen and simvastatin as the combination therapy for the treatment of hormonal dependent breast cancer cells. Toxicol Rep. 2019;6:1114–26.
10. Pinkerton JV. Selective estrogen receptor modulators in gynecology practice. Clin Obstet Gynecol. 2021;64(4):803–12. https://doi.org/10.1097/GRF.0000000000000647.
11. Barani M, et al. Evaluation of carum-loaded niosomes on breast cancer cells: physicochemical properties, in vitro cytotoxicity, flow cytometric, DNA fragmentation and cell migration assay. Sci Rep. 2019;9(1):1–10.
12. Birgani NB. Effect of carboplatin loaded niosomal nanoparticles on ovarian cancer cells. EC Pharmacol Toxicol. 2018;6:423–8.
13. Morello KC, Wurz GT, DeGregorio MW. Pharmacokinetics of selective estrogen receptor modulators. Clin Pharmacokinet. 2003;42:361–72.
14. Grilli G. Tamoxifen (TAM): the dispute goes on. Ann Ist Super Sanita. 2006;42(2):170.
15. Farrar MC, Jacobs TF. Tamoxifen. 2021 Jul 19. In: StatPearls [Internet]. Treasure Island (FL): StatPearls Publishing; 2022.
16. Herrscher H, Leblanc J, Petit TJBC. Agranulocytosis induced by tamoxifen in a breast cancer patient. Breast Care. 2020;15(1):72–4.
17. Makvandi P, et al. Drug delivery (nano) platforms for oral and dental applications: tissue regeneration, infection control, and cancer management. Adv Sci (Weinh). 2021;8(8):2004014.
18. Patra JK, et al. Nano based drug delivery systems: recent developments and future prospects. J Nanobiotechnology. 2018;16(1):71.
19. Shad PM, Karizi SZ, Javan RS, Mirzaie A, Noorbazargan H, Akbarzadeh I, Rezaie H. Folate conjugated hyaluronic acid coated alginate nanogels encapsulated oxaliplatin enhance antitumor and apoptosis efficacy on colorectal cancer cells (HT29 cell line). Toxicol in Vitro. 2020;65:104756.
20. Heydari Sheikh Hossein H, et al. Functionalization of magnetic nanoparticles by folate as potential MRI contrast agent for breast cancer diagnostics. Molecules. 2020;25(18):4053.
21. Boran G, et al. Synergistic effect of graphene oxide and zoledronic acid for osteoporosis and cancer treatment. Sci Rep. 2020;10(1):1–12.
22. Delfi M, et al. Self-assembled peptide and protein nanostructures for anti-cancer therapy: targeted delivery, stimuli-responsive devices and immunotherapy. Nano Today. 2021;38:101119.
23. Makvandi P, et al. Gum polysaccharide/nanometal hybrid biocomposites in cancer diagnosis and therapy. Biotechnol Adv. 2021;48:107711.
24. Day CM, et al. Novel tamoxifen nanoformulations for improving breast cancer treatment: old wine in new bottles. Molecules. 2020;25(5):1182.
25. Molani S, Madadi M, Wilkes WJO. A partially observable Markov chain framework to estimate overdiagnosis risk in breast cancer screening: incorporating uncertainty in patients adherence behaviors. Omega. 2019;89:40–53.
26. Akbarzadeh I, et al. Preparation, optimization and in-vitro evaluation of curcumin-loaded niosome@ calcium alginate nanocarrier as a new approach for breast cancer treatment. Biology (Basel). 2021;10(3):173.
27. Moghaddam FD, et al. Delivery of melittin-loaded niosomes for breast cancer treatment: an in vitro and in vivo evaluation of anti-cancer effect. Cancer Nanotechnol. 2021;12(1):1–35.
28. Amale FR, et al. Gold nanoparticles loaded into niosomes: A novel approach for enhanced antitumor activity against human ovarian cancer. Adv Powder Technol. 2021;32(12):4711–22.
29. Targhi AA, et al. Synergistic effect of curcumin-Cu and curcumin-Ag nanoparticle loaded niosome: enhanced antibacterial and anti-biofilm activities. Bioorg Chem. 2021;115:105116.
30. Moghtaderi M, et al. Enhanced antibacterial activity of Echinacea angustifolia extract against multidrug-resistant Klebsiella pneumoniae through niosome encapsulation. Nanomaterials (Basel). 2021;11(4):1573.
31. Jamshidifar E, et al. Super magnetic niosomal nanocarrier as a new approach for treatment of breast cancer: a case study on SK-BR-3 and MDA-MB-231 cell lines. Int J Mol Sci. 2021;22(15):7948.
32. Mirzaie A, Peirovi N, Akbarzadeh I, Moghtaderi M, Heidari F, Yeganeh FE, Noorbazargan H, Mirzazadeh S, Bakhtiari R. Preparation and optimization of ciprofloxacin encapsulated niosomes: a new approach for enhanced antibacterial activity, biofilm inhibition and reduced antibiotic resistance in ciprofloxacin-resistant methicillin-resistance Staphylococcus aureus. Bioorg Chem. 2020;103:104231.
33. Ghafelehbashi R, Akbarzadeh I, Tavakkoli Yaraki M, Lajevardi A, Fatemizadeh M, Heidarpoor Saremi L. Preparation, physicochemical properties, in vitro evaluation and release behavior of cephalexin-loaded niosomes. Int J Pharm. 2019;569:118580.
34. Barani M, et al. Lawsone-loaded niosome and its antitumor activity in MCF-7 breast cancer cell line: a nano-herbal treatment for cancer. Daru. 2018;26(1):11–7.
35. Hajizadeh MR, et al. In vitro cytotoxicity assay of D-limonene niosomes: an efficient nano-carrier for enhancing solubility of plant-extracted agents. Res Pharm Sci. 2019;14(5):448.
36. Ch MH, et al. Niosome-encapsulated tobramycin reduced antibiotic resistance and enhanced antibacterial activity against multidrug-resistant clinical strains of Pseudomonas aeruginosa. J Biomed Mater Res A. 2021;109(6):966–80.
37. Rasul A, et al. In vitro characterization and release studies of combined nonionic surfactant-based vesicles for the prolonged

delivery of an immunosuppressant model drug. Int J Nanomedicine. 2020;15:7937.
38. Tila D, et al. pH-sensitive, polymer modified, plasma stable niosomes: promising carriers for anti-cancer drugs. EXCLI J. 2015;14:21.
39. Khannazer N, Paylakhi SH, Mirshafiey A, Azizi G, Motamed N. Silibinin, up-regulates chemokine receptor expression in MDA-MB-231 breast cancer cell line. Bangladesh J Medical Sci. 2015;14(2):190–5.
40. Khan R, Irchhaiya R. An overview on niosomes as efficient drug carriers. Int J Pharm Biosci. 2017;8:106–16.
41. Muzzalupo R, Tavano L. Niosomal drug delivery for transdermal targeting: recent advances. Res Rep Transdermal Drug Deliv. 2015;4:23.
42. Khindri S, Aggarwal G. Role of niosomes and proniosomes for enhancing bioavailability of drugs. J Drug Deliv Ther. 2015;5(1):28–33.
43. Akbarzadeh I, et al. Niosomal formulation for co-administration of hydrophobic anticancer drugs into MCF-7 cancer cells. Arch Adv Biosci. 2020;11(2) https://doi.org/10.22037/aab.v11i2.28906.
44. Rochdy Haj-Ahmad R, Elkordy AA, Chaw CS. In vitro characterisation of Span™ 65 niosomal formulations containing proteins. Curr Drug Deliv. 2015;12(5):628–39.
45. Li Q, Li Z, Zeng W, Ge S, Lu H, Wu C, Ge L, Liang D, Xu Y. Proniosome-derived niosomes for tacrolimus topical ocular delivery: in vitro cornea permeation, ocular irritation, and in vivo anti-allograft rejection. Eur J Pharm Sci. 2014;62:115–23.
46. Basiri L, Rajabzadeh G, Bostan A. α-Tocopherol-loaded niosome prepared by heating method and its release behavior. Food Chem. 2017;221:620–8.
47. Kassem MA, el-Sawy HS, Abd-Allah FI, Abdelghany TM, el-Say KM. Maximizing the therapeutic efficacy of imatinib mesylate–loaded niosomes on human colon adenocarcinoma using Box-Behnken design. J Pharm Sci. 2017;106(1):111–22.
48. Patel J, Ketkar S, Patil S, Fearnley J, Mahadik KR, Paradkar AR. Potentiating antimicrobial efficacy of propolis through niosomal-based system for administration. Integr Med Res. 2015;4(2):94–101.
49. Bragagni M, Mennini N, Furlanetto S, Orlandini S, Ghelardini C, Mura P. Development and characterization of functionalized niosomes for brain targeting of dynorphin-B. Eur J Pharm Biopharm. 2014;87(1):73–9.
50. Moghassemi S, Hadjizadeh A. Nano-niosomes as nanoscale drug delivery systems: an illustrated review. J Control Release. 2014;185:22–36.
51. Sadeghi S, Bakhshandeh H, Ahangari Cohan R, Peirovi A, Ehsani P, Norouzian D. Synergistic anti-staphylococcal activity of niosomal recombinant lysostaphin-LL-37. Int J Nanomedicine. 2019;14:9777–92.
52. Barani M, Mirzaei M, Torkzadeh-Mahani M, Nematollahi MH. Lawsone-loaded niosome and its antitumor activity in MCF-7 breast cancer cell line: a nano-herbal treatment for cancer. DARU J Pharm Sci. 2018;26(1):11–7.
53. Hajizadeh MR, Maleki H, Barani M, Fahmidehkar MA, Mahmoodi M, Torkzadeh-Mahani M. In vitro cytotoxicity assay of D-limonene niosomes: an efficient nano-carrier for enhancing solubility of plant-extracted agents. Res Pharm Sci. 2019;14(5):448–58.
54. Alemi A, Zavar Reza J, Haghiralsadat F, Zarei Jaliani H, Haghi Karamallah M, Hosseini SA, Haghi Karamallah S. Paclitaxel and curcumin coadministration in novel cationic PEGylated niosomal formulations exhibit enhanced synergistic antitumor efficacy. J Nanobiotechnology. 2018;16(1):28.
55. Sadeghi S, Ehsani P, Cohan RA, Sardari S, Akbarzadeh I, Bakhshandeh H, Norouzian D. Design and physicochemical characterization of lysozyme loaded niosomal formulations as a new controlled delivery system. Pharm Chem J. 2020;53:1–10.
56. Salem HF, et al. Evaluation and optimization of pH-responsive niosomes as a carrier for efficient treatment of breast cancer. Drug Deliv Transl Res. 2018;8(3):633–44.
57. Manosroi A, Bauer K. The entrapment of a human insulin-DEAE dextran complex in different compound liposomes. Drug Dev Ind Pharm. 1989;15(14-16):2531–46.
58. Ag Seleci D, Seleci M, Walter JG, Stahl F, Scheper T. Niosomes as nanoparticular drug carriers: fundamentals and recent applications. J Nanomater. 2016;2016:**1**–**13**.
59. Kanaani L. Effects of cisplatin-loaded niosomal nanoparticleson BT-20 human breast carcinoma cells. Asian Pac J Cancer Prev: APJCP. 2017;18(2):365–8.
60. Yazdi Rouholamini SE, Moghassemi S, Maharat Z, Hakamivala A, Kashanian S, Omidfar K. Effect of silibinin-loaded nano-niosomal coated with trimethyl chitosan on miRNAs expression in 2D and 3D models of T47D breast cancer cell line. Artif Cells Nanomed Biotechnol. 2018;46(3):524–35.